Research Note
23rd International Meshing Roundtable (IMR23)

Determination of Flow Regions for Hybrid Grid Adaptation

Yannis Kallinderis[a,*], Vasileios Sassanis[a]

[a]*Laboratory of Aerodynamic Design of Air Vehicles, Department of Mechanical and Aeronautical Engineering, University of Patras, 26504 Rio, Greece*

Abstract

Adaptive grid refinement/coarsening is an important method for achieving increased accuracy of flow simulations with reduced computing resources. A primary issue of adaptive simulations is the reliable detection of the grid elements to be refined/coarsened. Various sensors for adaptation are employed via a spectrum of flow cases which include boundary layers (attached and separated), wakes, vortices, as well as shock waves. Two developments are presented regarding automation and effectiveness of the adaptation process. The first is automatic determination of a suitable threshold of local refinement/coarsening. The second involves a special adaptive octree technique that yields compact local adaptation regions.

Keywords: Flow feature detection; Grid adaptation; Hybrid grid

1. Introduction

Grid adaptation via local grid refinement/coarsening is an important method for achieving increased accuracy of flow simulations with reduced computing resources [1-3]. A major issue of adaptive simulations is the automatic and reliable determination of the regions of the grid that are to be refined/coarsened.

The problems of detection include (i) universality of application of the adaptation detection criteria (sensors) to a wide spectrum of flow fields and grids, (ii) the complete coverage of the appropriate regions, (iii) the resulting adapted mesh to be compact without local gaps or jaggedness of the boundaries of the detected zones, and (iv) the complexity and computational expense of application of adaptation sensors in particular for general hybrid grids in three dimensions.

* Corresponding author.
E-mail address: kallind@otenet.gr (Yannis Kallinderis), sassanisv@gmail.com (Vasileios Sassanis)

Previous work on adaptation criteria can be categorized as (i) field feature-based [e.g. 4, 5], and (ii) numerical error-based [e.g. 6]. Significant previous work exists on flow features detection. Some of those methods can be quite expensive involving calculation of eigenvalues and applicable only to structured grids. Employment of hybrid meshes consisting of prisms, hexahedra, tetrahedra, and pyramids poses an additional requirement on the sensors to be relatively simple.

Various sensors based on the flow quantities are employed and evaluated via a spectrum of flow cases which include boundary layers, both attached and separated, wakes, vortices and shock waves. Emphasis is placed on the common characteristics of the sensors distributions, which can lead to a reliable determination of a suitable threshold for adaptation.

The issues of complete coverage of the appropriate regions, as well as the compactness at the adaptation regions (i.e. no holes and non-jagged boundaries), exist for all the above methods, both the flow feature-based and the numerical error-based ones. Work aimed at the "regularization" of the detected zones for adaptation by manipulating (post-processing) the related data have been reported in [7]. It is practically very difficult to have regular adaptation regions due to numerical noise, transients, incomplete convergence, weak features etc. Therefore, work on this area of automatic post-processing of the detected regions is important and it is a focus of the present work.

2. Flow features detection

Adaptation of general hybrid grids consisting of prisms, hexahedra, tetrahedra and pyramids "favors" relatively simple formulations of the sensors. The sensors are based on the flow quantities. Those quantities are cast into simple mathematical forms that express spatial variation. Specifically, first order differences (Δq) and corresponding derivatives $(\Delta q/\Delta S)$ of the flow quantities (q) along the edges joining the centers of the neighboring grid elements of length (ΔS) are considered. The flow quantities (q) include the total velocity (U) and its direction (θ), pressure (P), and the Mach number. This is not a complete set of possible sensors. Nevertheless, it includes some popular ones.

The suitability of each sensor to capture boundary layers, vortices, and shock waves is examined in this section. Those features appear distinctly in the chosen flow field cases and are good tests to judge the effectiveness of the sensors employed, namely the first order spatial differences and gradients of pressure, total velocity magnitude and velocity direction. The hybrid grids were generated via the CENTAUR mesh generator [8].The flow simulations were performed using the Open FOAM open source code [9].

The case of incompressible flow around a sphere at Re = 40 includes multiple flow features. Distinct capture of the boundary layer in the presence of the wake and vortices is an issue to examine. Fig. 1(a) illustrates the hybrid mesh used. It is observed in Fig. 1(b) that distinct capture of the attached boundary layer is afforded by the velocity gradients sensor ($\Delta U/\Delta S$).

The case of the flow around a cylinder at Re = 170 exhibits strong detached vortices that are shed from the cylinder. Detection of those vortices in the presence of the attached boundary layer and the wake is of interest. The change in velocity direction $(\Delta\theta)$ appears effective in capturing the shed vortices distinctly as illustrated in Fig. 2(a).

A distinct bow shock wave is the main feature of the case of supersonic flow around a sphere. It is an interesting type of shock as it exhibits a strong central part and weakens on the sides as it becomes oblique. The grid resolution is not sufficient to capture the attached portion of the boundary layer at this high Reynolds number of 10^7. The pressure differences sensor, shown in Fig. 2(b), performs very well, as expected, in capturing the bow shock distinctly. The central and the oblique parts of the feature are detected, while the rest of the flow features are ignored by this sensor.

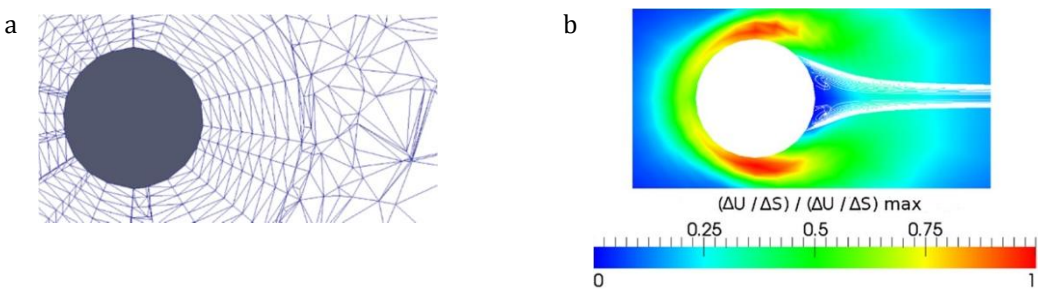

Fig. 1. Case of flow around a sphere: (a) Planar cut of the hybrid mesh used; (b) values of the sensor based on velocity gradients (ΔU / ΔS).

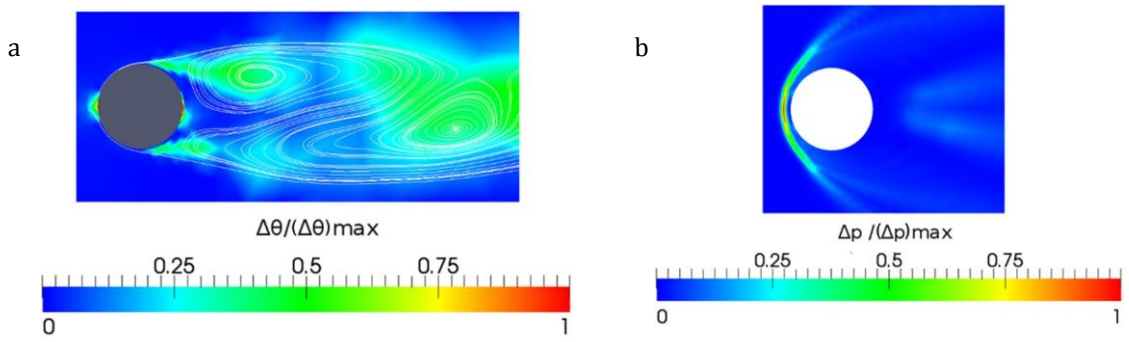

Fig. 2. (a) Values of the sensor based on velocity direction change (Δθ) for the case of flow around a cylinder; (b) values of the pressure-based sensor (Δp) for the case of supersonic flow past a sphere.

3. Adaptation threshold

This section deals with a difficult and yet critical problem, namely the determination of the threshold values of the sensors for adaptive refinement/coarsening. Typically, local refinement is applied where the sensor is above a certain value (threshold). Also, previous refinement is removed where the sensor falls below another threshold value.

The present work starts with a comparative study of the sensors distributions for the flow cases considered. The flow cases are: (i) cylinder (Re = 170), (ii) flat plate (Re = 300), (iii) subsonic duct (Re = 200), (iv) sphere (Re = 40), (iv) supersonic sphere (Re = 1E+07, Ma = 2.4), (v) supersonic duct (Re = 1E+07, Ma = 2.4) and (vi) aircraft (Re = 5E+07, Ma = 0.3, AoA = 15º). Fig. 3(a) illustrates the distributions of the velocity differences sensor normalized by its maximum value. The shapes of the distributions are quite similar which will facilitate definition of a suitable threshold for refinement. The shape of the distributions for cases simulated with coarse and their globally-refined counterparts is preserved as shown in Fig. 3(b) for the sensor based on velocity direction change. Similar behaviour is observed for the rest of the sensors.

Next, the similarities of the distributions are examined quantitatively. Besides the average and standard deviation of the distribution curves, two shape parameters will be employed, namely the *skewness* and the *kurtosis*. *Skewness* is defined as: $\gamma_1 = \mu_3 / \sigma^3$, while *kurtosis* is defined as $\beta_2 = \mu_4 / \sigma^4$. In the aforementioned expressions, σ is the *standard deviation* of a distribution (x) with number of elements *(n)* and a *mean value* of $\bar{x}$, while μ_i denotes the *i-th central moment* of the distribution and is given as $\mu_i = \frac{1}{n}\sum_{j=1}^{n}(x_j - \bar{x})^i$. The distributions have at most high, positive *skewness*. This homogeneity of the distributions is very helpful for the threshold definition.

Due to the observed regularity and commonality of the shapes of the sensor distributions, a "universal" threshold for grid adaptation can be established. The value where the distribution line "bends" is sought after. Specific formula of the adaptation threshold (T) is proposed in the present work:

$$T = \bar{x} - \alpha \cdot \sigma \tag{1}$$

with $\alpha = \beta_2/(10 \cdot |\gamma_1|)$ for $|\gamma_1| \geq 1$ and $\alpha = 1$ for $0 \leq |\gamma_1| \leq 1$.It is noted that the threshold coefficient (α) is smaller than 1 for highly skewed distributions. It has been observed that (α) has remarkably stable values, namely α=1 for small skewness curves, while a value of (α) of about 0.3 could be acceptable for higher skewness distributions.

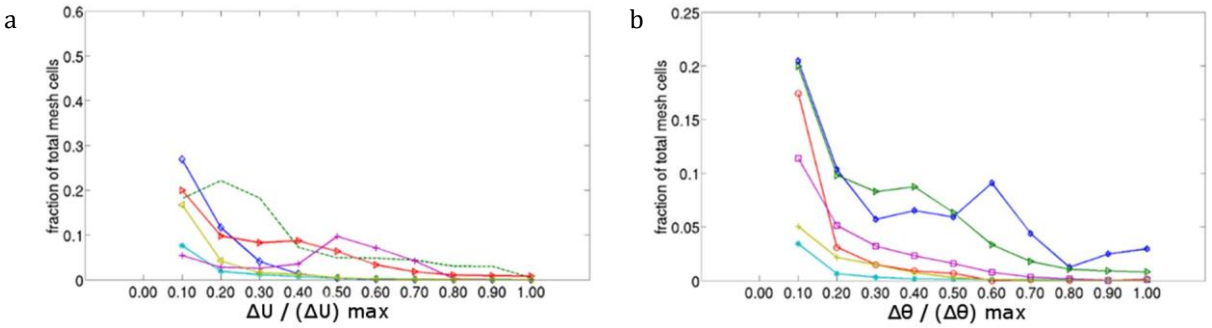

Fig. 3.(a) Distributions of the sensor based on velocity differences (ΔU) for the following flow cases: cylinder (◊), flat plate (--), sphere (fine mesh) (▷), supersonic sphere (fine mesh) (✳), supersonic duct (fine mesh) (+), aircraft (◁); (b) distributions of the sensor based on velocity direction change (Δθ) between *coarse* and *globally-refined* meshes for the following cases: sphere (coarse mesh) (✱), sphere (fine mesh) (▷), supersonic sphere (coarse mesh) (○), supersonic sphere (fine mesh) (✳), supersonic duct (coarse mesh) (□), supersonic duct (fine mesh) (+).

4. An automatic technique for compact adaptation regions

Application of any sensor for grid adaptation does not always result in a complete coverage of the regions where flow features exist. That is, part of the feature of interest might be missed. Also, "holes" of undetected areas may exist. Fig. 4(a) depicts the elements that are flagged for refinement in the regions of an oblique shock wave that reflects on the upper wall of the duct in supersonic flow. Those elements are denoted in red color. Sparse coverage of the areas of the oblique shocks is observed in this manufactured case.

A special technique is proposed in the present work in order to post-process the initial flags of the sensor and enhance (expand and fill-in the gaps) the adaptation regions. It is based on the employment of a special octree which "detects" the flagged regions and automatically refines itself in those regions. The octants kept for further refinement are the ones that contain at least one flagged element. Fig. 4(b) depicts the octree that is automatically constructed. It is observed that this special octree follows the oblique shocks structure quite faithfully.

The "regularization" of the flagged zones is achieved via flagging the octants rather than grid elements. Then, all elements within or intersecting such a flagged octant are flagged for adaptation (refinement or coarsening). Those octants belong to the locally finest level of the octree and they are flagged if the percentage of the flagged grid elements they contain exceeds a specific value.

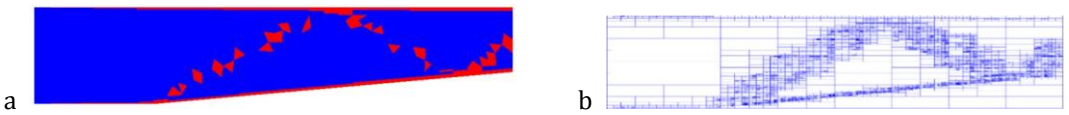

Fig. 4. Case of the supersonic ducted flow (Re = 1E+07, Ma = 2.4): (a) Cells flagged for adaptive refinement in the boundary layer and shock regions using the sensor based on velocity differences (ΔU); (b) the corresponding spatial decomposition via the octree technique using the flags of the sensor.

There are two parameters that need to be determined when applying the above octree technique. The first is the size of the octants at the finest level, while the second is the percentage of flagged grid elements associated with each flagged octant above which *all* associated elements are flagged for adaptation.

Let $V_{mesh,min}$, $V_{mesh,aver}$ *and* $V_{mesh,max}$ be the minimum, average and maximum element volume, respectively in a given mesh. The octree technique subdivides an initial cube into eight octants of equal volumes at each division level. If $V_{cube,initial}$ is the volume of the initial cube surrounding a given mesh and d is the depth of division, then, the volume of each octant (V_{oct}) at this depth will be: $V_{oct} = V_{cube,initial} / 8^d$. The average volume of each mesh element in an octant ($V_{cell,aver}$) is approximated by $V_{cell,aver} = 0.5 \cdot (V_{mesh,aver} + V_{mesh,min})$.

The depth (d) of division in a given mesh is approximated empirically as: $d = 0.5 \cdot V_{mesh,max}$. The number of mesh elements contained in an octant at a depth d of division will be $V_{cube,initial} / (8^d \cdot V_{cell,aver})$. If the percentage of flagged elements contained in an octant is above 10% of the octant's elements, then all the octant's elements are flagged for adaptation.

The case of the supersonic flow past a sphere with Mach number of 2.4 and Reynolds number of 10^7 is used to demonstrate application of the special octree in order to capture shock wave and wakes in a complete and compact way. It should be noted that the hybrid grid employed does not resolve the very thin boundary layer and is intended for the bow shock and the wake. The initial flagged elements are shown in Fig. 5(a). It is observed that the two features that are detected, namely the bow shock and the far wake are captured relatively weakly. Application of the special octree results in the final flagging of Fig. 5(b). Both features are now captured more completely. Furthermore, the observed "holes" of the initial flags have disappeared.

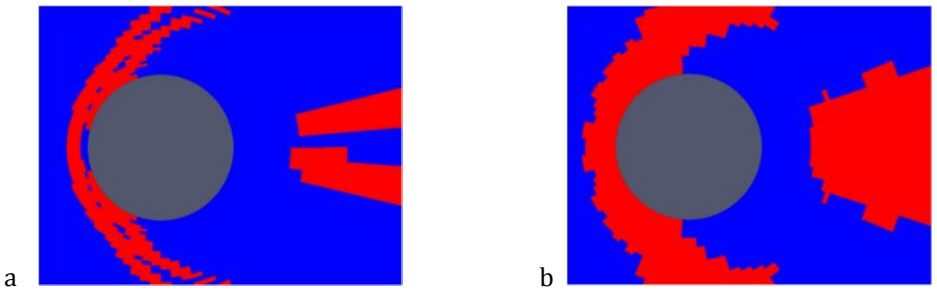

Fig. 5. Effect of the octree technique on compactness of the adaptation region. Case of the supersonic flow past a sphere (Re = 1E+07, Ma = 2.4): (a) Initial flagging of cells for refinement; (b) final flags after application of the special octree.

5. Summary and conclusion

Grid adaptation sensors were examined. They were based on the flow quantities of pressure, velocity (both magnitude and direction). Both spatial differences and gradients were considered. They were applied to flow field cases that included boundary layers, wakes, vortices, and shock waves.

The shapes of the sensors distributions were remarkably similar. This was also the case when comparing fine and coarse meshes for the same flow. As a result, a relatively simple determination of a general threshold for adaptive refinement was devised.

Lastly, a special adaptive octree was presented aimed at regularizing the local regions flagged for adaptation. The octree was constructed based on the flagged grid elements and proved quite effective in yielding adaptation regions that covered the flow features completely and without gaps.

Future work will focus on a more complete set of sensors along with a quantitative measure of their coverage of flow feature regions.

References

[1] Y. Kallinderis (Ed.), Adaptive methods for compressible CFD, Computer Methods in Applied Mechanics and Engineering, Special Issue 189(2), 2000.

[2] J.C. South Jr., J.L. Thomas, J. Van Rosendale (Eds.), ICASE/LaRC Workshop on adaptive grid methods, NASA Conference Publication 3316, 1995.

[3] Y. Kallinderis, C. Kavouklis, A dynamic adaptation scheme for general 3D hybrid meshes, Computer Methods in Applied Mechanics and Engineering, 194 (2005) 5019-5050.

[4] N. Kasmai, D. Thompson, E. Luke, M. Jankun-Kelly, R. Machiraju, Feature-based adaptive mesh refinement for wingtip vortices, International Journal for Numerical Methods in Fluids, 66 (2011) 1274-1294.

[5] D. Lovely, R. Haimes, Shock detection from computational fluid dynamics results, Paper AIAA 3285, 1999.

[6] H.J. Kim, K. Nakahashi, Output-based error estimation and adaptive mesh refinement using viscous adjoint method, Paper AIAA 1395, 2006.

[7] D. Marcum, K. Gaither, Solution adaptive unstructured grid generation using pseudo-pattern recognition techniques, Paper AIAA 1860, 1997.

[8] CENTAUR Software - Computational Grids for Advanced Modelling. *www.centaursoft.com.*

[9] OpenFOAM - The Open Source CFD Toolbox. *www.openfoam.com.*